IUST
Iran University of Science and Technology

Iranian Journal of Electrical and Electronic Engineering

Journal Homepage: ijeee.iust.ac.ir

Research Paper

Sliding Mode and Terminal Sliding Mode Control of Cascaded Doubly Fed Induction Generator

H. Zahedi Abdolhadi*, Gh. Arab Markadeh*(C.A.), and S. Taghipour Boroujeni*

Abstract: Classical structure of Doubly Fed Induction Generators (DFIGs) is not completely adapted in high-speed regions due to their brushes and slip rings. So in the Cascaded DFIGs (CDFIGs), the rotor windings of a given DFIG are supplied by another wound rotor induction machine leading to a complete brushless structure. This paper presents and compares Sliding Mode Control (SMC) and Terminal Sliding Mode Control (TSMC) methods to control the output voltage of CDFIG. The SMC and TSMC methods are identified as strong controllers with large stability and robustness margins. In this paper, the SMC and TSMC methods are evaluated and compared to the conventional Voltage Oriented Control (VOC) in terms of output voltage change, prime over speed's variation, and nonlinear load. Simulation and experimental results using a TMS320F28335 based prototype system show that the SMC and TSMC techniques are more robust against parameter variations and uncertainties, and TSMC offers improved dynamic response.

Keywords: CDFIG, SMC, TSMC, CDFIG, Nonlinear Load.

1 Introduction

THE energy problem is an important issue in human society. Great deals of effort are continually made to address this problem. The idea of smart energy grids based on high-level integration of renewable energy sources has, therefore, come to the spotlight.

Variable speed constant frequency (VSCF) operation is used in many industries that require Doubly Fed Induction Generators (DFIG) [1]. In these generators, even if there is a change of speed, they can be directly connected to the constant frequency grid using partially rated converters and rotor current regulation. Therefore, they are useful for use in wind and hydropower systems [2].

However, the structure of these generators, which includes brushes and slip rings, reduces the life of the device due to the need for maintenance. Therefore, it is not quite suitable for use in applications such as aircraft, which require high reliability and long maintenance period. In the CDFIG generator, by using two DFIGs and connecting the windings of the rotors to each other, a new brushless structure is obtained, which can be a suitable alternative to DFIG [3]. CDFIG works like a single DFIG so it can be connected directly to the network.

By connecting the two DFIG rotors mechanically and electrically, a CDFIG is obtained. DFIG machines are known as power machine and control machine [4]. The electric load or the grid is connected to the stator winding of the power machine (PM), and a power electronic converter supplies the stator winding of the control machine [5], Fig. 1.

Several studies on variable speed constant frequency generating system (VSCF) using CDFIG have been

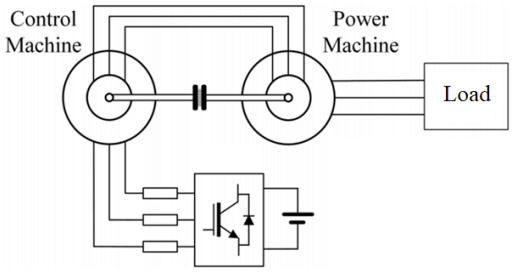

Fig. 1 CDFIG configuration.

Iranian Journal of Electrical and Electronic Engineering, 2021.
Paper first received 10 August 2020, revised 14 October 2020, and accepted 17 October 2020.
* The authors are with the Electrical Engineering Department, Faculty of Technology, Shahrekord University (SKU), Shahrekord, Iran.
E-mails: zahedi13@gmail.com, arab-gh@eng.sku.ac.ir, and s.taghipour@sku.ac.ir.
Corresponding Author: Gh. Arab Markadeh.
https://doi.org/10.22068/IJEEE.17.3.1955

performed in applications such as windmills, hydropower, and aircraft power supply [6].

The structure of CDFIG is complex in architecture and difficult to control, as well as, de-rating of the machine and higher price in comparison with DFIG. Therefore, despite its advantages, it is not widely used. Due to the large size of the dynamic equation model, which is obtained by merging two DFIGs, the control of this machine has been influenced by its architecture [7]. A vector control method for DFIG is proposed in [8, 9]. Also, an improved direct vector control based on SVM for DFIG is studied in [10]. The method of improving the stability of multi-machine power network (MMPN) has been studied and the application of the conventional non-linear sliding mode control (SMC) is presented in [11].

The terminal SMC as a modified version of the conventional sliding mode control is presented in [12] for DFIG. Reference [13] is focused on the control algorithm of DFIG system based on the sliding mode approach and rotor position estimation. In [14] a second-order sliding mode control strategy using an artificial neural network on the rotor side converter of a DFIG is applied.

Efforts to control CDFIG have been limited, mainly based on field-oriented control or vector control. In the vector control method, linear controllers such as PI regulate the components of the rotor currents, which include torque (or active power) and rotor flux (or reactive power). [15, 16].

In [17], the active and reactive power of the power machine is controlled based on vector control using PI controllers. But in this method, all machine parameters are required in a recursive structure to generate the rotor reference currents and then the control machine reference currents. Also, CDFIG is controlled based on DPC for wind energy applications in [18].

A disadvantage of the SMC is its low convergence rate as a result of using a linear sliding surface. To improve the convergence rate in a linear sliding mode, controller gains need to increase substantially. However, this can cause saturation under the effect of the input signal [19-21]. In terminal sliding mode controller (TSMC) which is based on a nonlinear terminal sliding surface, system responses converge in a shorter time [22, 23].

In this paper, the objective is to apply the SMC and TSMC to CDFIG and investigate the system responses for potential use in the renewable energy system network. First, the generator is introduced and modeled. Then, the VOC as well as the SMC and TSMC techniques are studied and applied. Their simulation and practical results are presented and compared. Improved robustness properties of the sliding mode control method and also the improvement of the transient responses offered by the TSMC are observed and confirmed.

2 Study System Description and Mathematical Model

Fig. 1 shows the general interface of a CDFIG with isolated load or in islanded AC microgrid. As can be seen, the control machine is supplied by a three-phase inverter and the power machine is connected to three-phase load.

The two DFIMs have pole pair p_1 and p_2 respectively, with rotors connected in inverse coupling sequence. Then the voltages and currents of rotors can be written as:

$$\begin{aligned} v_{qr} &= v_{qr1} = v_{qr2} \\ v_{dr} &= v_{dr1} = -v_{dr2} \\ i_{qr} &= i_{qr1} = -i_{qr2} \\ i_{dr} &= i_{dr1} = i_{dr2} \end{aligned} \tag{1}$$

where v_{qr}, v_{dr}, i_{qr}, and i_{dr} are the rotor voltage and rotor current components, respectively. In order to avoid all ambiguity between the two DFIM of the cascade, 1 and 2 subscripts will be employed for all quantities in the system.

The subscripts *s* or *r* show the quantities of stator or rotor, and number 1 or 2 show the parameters of power or control machine, and q or d show the quantities of q-component or d-components, respectively.

Let the rotor be rotating at the mechanical angular frequency ω_m and the frequency of PM voltage is ω_1, the frequency of the induced flux into the rotor bars (ω_r) is equal to the slip frequency of the power machine,

$$\omega_r = \omega_1 - p_1 \bullet \omega_m \tag{2}$$

Since the phase sequence is reversed at the point of rotor connection, the frequency of flux wave due to the rotor control machine is opposite to the power machine slip frequency,

$$\omega_2 = -\left(\omega_1 - \left(p_1 + p_2\right) \bullet \omega_m\right) \tag{3}$$

In other words, ω_m can be shown as

$$\omega_m = \frac{\omega_1 + \omega_2}{p_1 + p_2} \tag{4}$$

The behavior of CDFIG can be described by equations for each stator and combination of rotors. The complete CDFIG dynamic model in d-q reference frame can be given as:

$$v_{qs1} = R_{s1} \bullet i_{qs1} + \frac{d}{dt}\lambda_{qs1} + \omega_1 \lambda_{ds1}$$

$$v_{ds1} = R_{s1} \bullet i_{ds1} + \frac{d}{dt}\lambda_{ds1} - \omega_1 \lambda_{qs1}$$

$$v_{qs2} = R_{s2} \bullet i_{qs2} + \frac{d}{dt}\lambda_{qs2} + \omega_2 \lambda_{ds2}$$

$$
\begin{aligned}
v_{ds2} &= R_{s2} \bullet i_{ds2} + \frac{d}{dt}\lambda_{ds2} - \omega_2 \lambda_{qs2} \\
v_{qr} &= R_r \bullet i_{qr} + \frac{d}{dt}\lambda_{qr} + \omega_r \lambda_{dr} \\
v_{dr} &= R_r \bullet i_{dr} + \frac{d}{dt}\lambda_{dr} - \omega_r \lambda_{qr}
\end{aligned} \tag{5}
$$

where R, v, i, and λ are the is the winding resistance, voltage, current, and flow of the control machine and power machine.

So, (5) can be written in matrix form as:

$$\dot{\Lambda} = V - R \bullet I - \Omega \bullet \Lambda \tag{6}$$

where

$$
\Lambda = \begin{bmatrix} \lambda_{qs1} \\ \lambda_{ds1} \\ \lambda_{qs2} \\ \lambda_{ds2} \\ \lambda_{qr} \\ \lambda_{dr} \end{bmatrix}, \quad V = \begin{bmatrix} v_{qs1} \\ v_{ds1} \\ v_{qs2} \\ v_{ds2} \\ v_{qr} \\ v_{dr} \end{bmatrix}, \quad I = \begin{bmatrix} i_{qs1} \\ i_{ds1} \\ i_{qs2} \\ i_{ds2} \\ i_{qr} \\ i_{dr} \end{bmatrix},
$$

$$
\begin{aligned}
R &= diag\begin{bmatrix} R_{s1} & R_{s1} & R_{s2} & R_{s2} & R_r & R_r \end{bmatrix}, \\
\Omega &= diag\begin{bmatrix} \omega_1 & \omega_1 & \omega_2 & \omega_2 & \omega_r & \omega_r \end{bmatrix}
\end{aligned} \tag{7}
$$

The stators and rotor flux vectors can be expressed as

$$\Lambda = L \cdot I \tag{8}$$

where

$$
L = \begin{bmatrix}
L_{ls1} & 0 & 0 & 0 & L_m & 0 \\
0 & L_{s1} & 0 & 0 & 0 & L_m \\
0 & 0 & L_{ls2} & 0 & -L_m & 0 \\
0 & 0 & 0 & L_{s2} & 0 & L_m \\
-L_m & 0 & L_m & 0 & -L_{lr} & 0 \\
0 & L_m & 0 & L_m & 0 & L_r
\end{bmatrix} \tag{9}
$$

Then by substituting (9) into (8) and rearrange the equations, (6) can be rewritten based on the derivations of currents.

The equivalent circuit of CDFIG is shown in Fig. 2.

3 Three Control Methods

In this section, three control methods including VOC, SMC, and TSMC are presented.

3.1 Voltage Oriented Control

In the VOC method, the coupling terms are removed and simple P or PI controllers are used for each decoupled loop. According to (5) and using the VOC method, the following controller can be obtained:

$$
\begin{aligned}
v_{qs2} &= K_{P.q} \bullet e_q(t) + K_{I.q} \bullet \int e_q(t)dt \\
v_{ds2} &= K_{P.d} \bullet e_d(t) + K_{I.d} \bullet \int e_d(t)dt
\end{aligned} \tag{10}
$$

where $K_{P.q}$, $K_{I.q}$, $K_{P.d}$, and $K_{I.d}$ are constant positive gains, and $e_q(t)$ and $e_d(t)$ are the differences between references and actual values of direct and quadrature output voltage, respectively.

$$
\begin{aligned}
e_q &= v_{qs1}^{ref} - v_{qs1} \\
e_d &= v_{ds1}^{ref} - v_{ds1}
\end{aligned} \tag{11}
$$

Therefore, the output voltage errors exponentially converge to zero. The complete structure of the VOC controller is shown in Fig. 3(a).

3.2 SMC

The SMC is recognized as a robust nonlinear controller that allows incorporating system nonlinearities and uncertainties into the design process. In the sliding mode control by selecting a sliding surface in the state space, if the motion is bounded to it, it will slide to the eligible point. Then a control law is designed to cause the state to reach the sliding surface.

The system state is transferred from an arbitrary initial state to the sliding surface (reaching mode) and, stay in the sliding surface forever (or close to it) and move to the equilibrium point (sliding state) [24]. A typical sliding surface candidate is defined as:

$$
S = \begin{bmatrix} S_q \\ S_d \end{bmatrix} = Kx_1 + x_2 = \begin{bmatrix} Ke_q + \int e_q(t)dt \\ Ke_d + \int e_d(t)dt \end{bmatrix} \tag{12}
$$

where $x_1.x_2$ and $K > 0$ are the tracking error, tracking error integral, and control parameter. If the following rule is satisfied, the reaching condition is guaranteed:

$$S\dot{S} \le 0 \tag{13}$$

The controller's structure consists of two parts.

$$u(t) = u_c(t) + u_d(t) \tag{14}$$

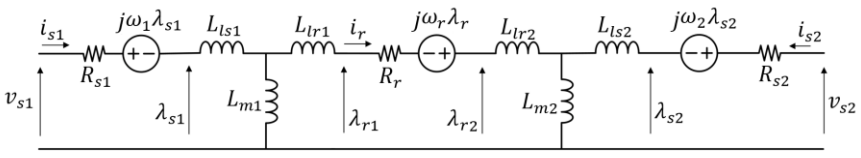

Fig. 2 Equivalent circuit of CDFIG.

where the parts $u_c(t)$ and $u_d(t)$ stand for continuous and discontinuous respectively. It should be noted that $u_d(t)$ employs the sign or saturation function. To apply the SMC method to the CDFIG, two sliding surfaces are defined as:

$$\begin{aligned} S_q &= e_q(t) + K_q \bullet \int e_q(t)dt \\ S_d &= e_d(t) + K_d \bullet \int e_d(t)dt \end{aligned} \tag{15}$$

When the system states achieve the desired surface, then we have:

$$\begin{aligned} S_q &= \dot{S}_q = 0 \\ S_d &= \dot{S}_d = 0 \end{aligned} \tag{16}$$

If the control laws are selected properly, we have

$$\begin{aligned} \dot{e}_q &= -K_q \bullet e_q \\ \dot{e}_d &= -K_d \bullet e_d \end{aligned} \tag{17}$$

It means that the errors will converge exponentially to zero. According to (17)

$$\begin{aligned} \dot{S}_q &= \dot{e}_q + K_q \bullet e_q \\ \dot{S}_d &= \dot{e}_d + K_d \bullet e_d \end{aligned} \tag{18}$$

Substituting (6) into (18) yields

$$\dot{S} = A \bullet X + B \bullet U + K \bullet e \tag{19}$$

By define $L_a = 2(L_r L_s – L_m^2)$, $L_b = 2L_r L_s – L_m^2$ and

$$\begin{aligned} A &= \frac{1}{L_a}\begin{bmatrix} -(Rs+RL)\times L_b / Ls & L_m^2 \times wm \\ -L_m^2 \times wm & (Rs+RL)\times L_b / Ls \\ L_m^2 \times Rs / Ls & L_m^2 \times wm \\ L_m^2 \times wm & L_m^2 \times Rs / Ls \\ L_m R_r & -L_m \times wm / L_s \\ -L_m \times wm / L_s & L_m R_r \end{bmatrix}^T, \\ B &= \frac{1}{L_a}\begin{bmatrix} L_m^2 \times RL / Ls & 0 \\ 0 & L_m^2 \times RL / Ls \end{bmatrix}, \\ K &= \begin{bmatrix} K_q & 0 \\ 0 & K_d \end{bmatrix}, \qquad e = \begin{bmatrix} v_{qs1}^{ref} - v_{qs1} \\ v_{ds1}^{ref} - v_{ds1} \end{bmatrix} \end{aligned} \tag{20}$$

where *RL* is the load resistance.

By applying Lyapunov theory in SMC method, the conditions of control law are derived and the state trajectory towards the desired behavior. Consider the quadratic function of Lyapunov as follows

$$W = \frac{1}{2} S^T S \tag{21}$$

The time derivative of *W* of (16) is expressed as

$$\dot{W} = \frac{1}{2}\left(S^T \dot{S} + \dot{S}^T S\right) \tag{22}$$

The control law should be selected so that the time derivative of W is negative definite with $S \neq 0$. Thus, the control law is selected as follow

$$\begin{bmatrix} v_{qs2} \\ v_{ds2} \end{bmatrix} = -B^{-1} \bullet \left(A + \begin{bmatrix} K_q \bullet \mathrm{sgn}(S_q) \\ K_d \bullet \mathrm{sgn}(S_d) \end{bmatrix} \right) \tag{23}$$

where K_q and K_d are positive control gains, sgn(S_q) and sgn(S_d) are switching functions for direct and quadrature of output voltage respectively.

In order to decrease the chattering phenomena, the discontinuous sign function can be replaced with saturation function. The reference voltage that is obtained from (23) can be used to drive the stator of the control machine. Fig. 3(b) shows the block diagram of SMC for this application.

3.3 TSMC

The TSMC design is based on selecting a nonlinear sliding surface causing the responses to converging more rapidly. The sliding surface in the TSMC is selected as (24) [22].

$$S = x_2 + K x_1^{q/p} \tag{24}$$

where *K* is positive and *p* and *q* are positive odd integer coefficients, such that $p > q$.

The sliding condition is selected as in (13). Substituting the time derivative of the terminal sliding mode function into (13) yields

$$S\left(\dot{x}_2 + K\frac{q}{p} x_1^{q/p - 1}\dot{x}_1\right) < 0 \tag{25}$$

It should be noted that the system dynamics on the sliding surface is given by $S = 0$ leading to

$$\dot{x}_1 = -K x_1^{q/p} \tag{26}$$

Therefore, the finite time for convergence is obtained as follows:

$$t_s = \frac{p}{K(p-q)}\left|x_1(0)\right|^{1-q/p} \tag{27}$$

Equation (27) indicates that the system state converges to zero within finite time. In fact, “terminal” refers to this property of the TSMC method [25]. It is noteworthy that the time t_s may be adjusted by *K*, *p*, and *q*. The term $x_1^{q/p}$ improves the convergence time. To apply the TSMC to the CDFIG, the sliding surfaces are defined as follows:

$$\begin{aligned} S_q &= e_q(t) + K_q \bullet \int e_q^{q/p}(t)dt \\ S_d &= e_d(t) + K_d \bullet \int e_d^{q/p}(t)dt \end{aligned} \tag{28}$$

According to the sliding surface selected in (28) and the sliding condition, the control law can be obtained by setting

$$\begin{aligned} S_q &= \dot{S}_q = 0 \\ S_d &= \dot{S}_d = 0 \end{aligned} \tag{29}$$

Similar to (12), by combining (22) and (24) yields:

$$\begin{bmatrix} v_{qs2} \\ v_{ds2} \end{bmatrix} = -B^{-1} \bullet \left(A + \begin{bmatrix} K_q \bullet \mathrm{sgn}(S_q) \\ K_d \bullet \mathrm{sgn}(S_d) \end{bmatrix} \right) \tag{30}$$

Fig. 3(c) shows the block diagram of the TSMC method.

4 Simulation and Experimental Results

In order to investigate the effectiveness of the proposed control methods, simulation and experimental results are obtained in three distinct conditions: 1) the output voltage reference changes, 2) change in rotor speed, and 3) load resistance uncertainty.

The simulations are performed in the MATLAB/Simulink software environment at the simulation time step of 20 µs. For the experimental evaluations, a DSP-based prototype is built and used. Fig. 4 shows the control block diagram.

The experimental setup of the overall system is shown in Fig. 5 which consists of a three-phase load, two cascaded DFIG with 370w, the sensor board, the signal conditioning circuit, and the TMS320F28335 discrete signal processor board.

Four Hall-effect current sensors (LEM LTS-6-NP) are measured the phase currents, and a voltage sensor (LEM LV-25P) is calculated the line-to-line voltage. The analog second-order low pass filters are used to filtered the measured stator currents and voltage signals, with cut-off frequency of about 2.6 kHz, and converted to digital by 12-bit on-chip A/D converters at 500ns conversion time.

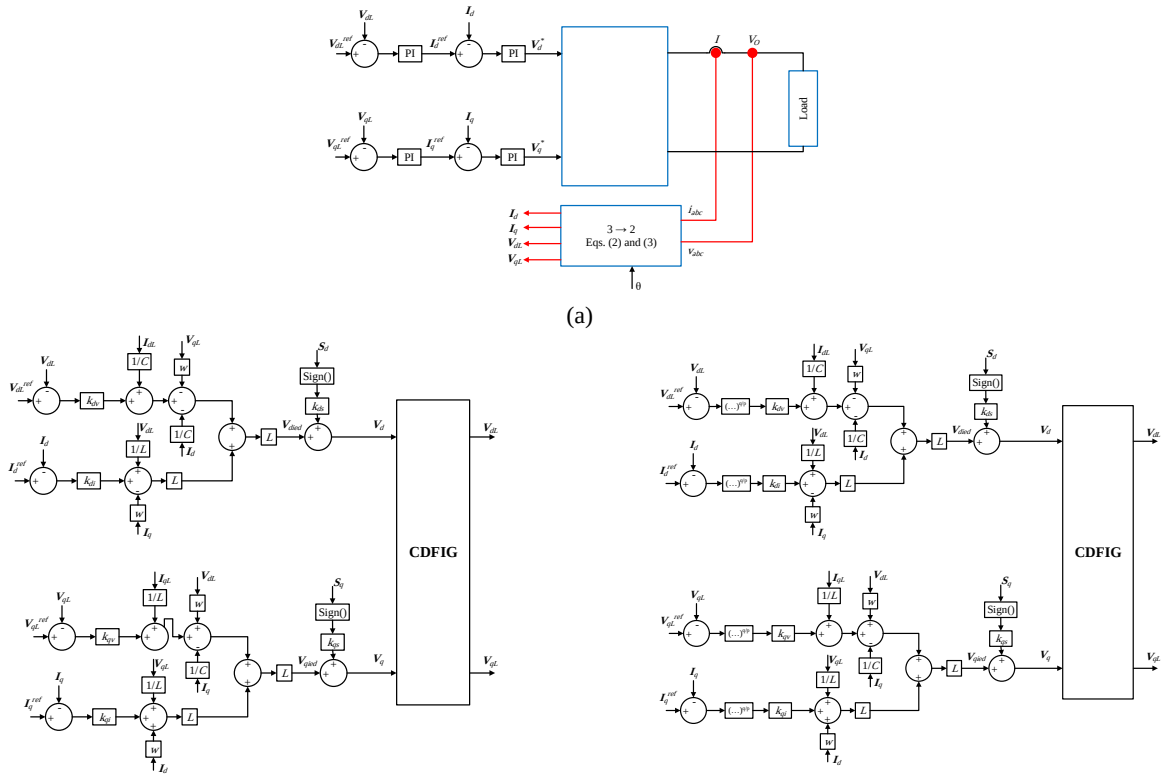

(a) (b) (c)

Fig. 3 Control system block diagrams: a) VOC method, b) SMC method, and c) TSMC method.

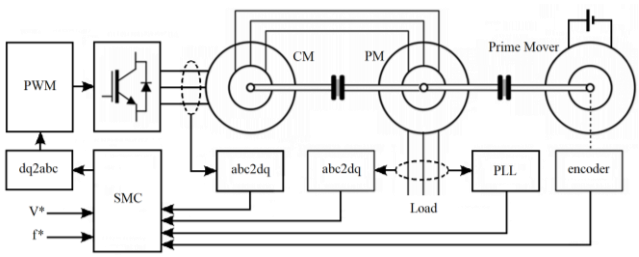

Fig. 4 Block diagram of SMC for CDFIG.

The inverter which is used to derive the control machine, is designed using the low-loss IGBT module SKM40GD124D (with 40 A, 1200 V ratings). Also, intelligent IGBT drivers, HCPL-316J, is used in this inverter which guarantees electrical separation between the power and control systems. The switching frequency of the inverter is selected as 10 kHz.

The machine parameters are listed in Table 1.

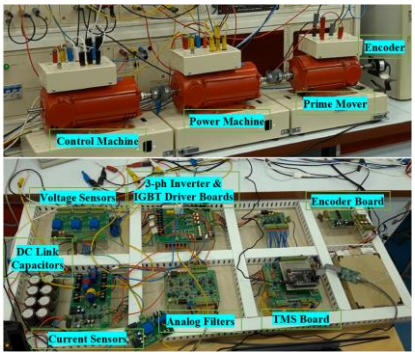

Fig. 5 Experimental setup.

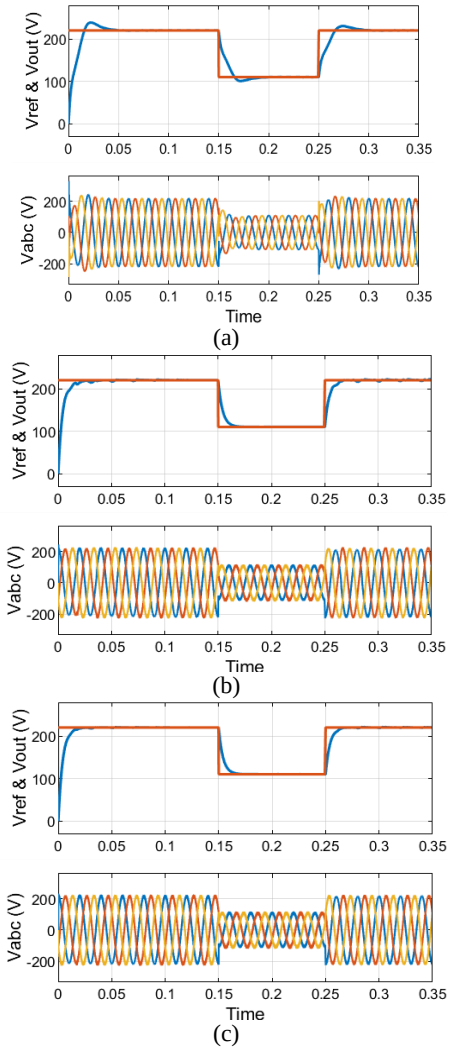

Fig. 6 Simulation results for the dynamic response to changes in the reference value, V_{ref} (red), V_{out} (blue), 3-phase voltage; a) VOC method, b) SMC method, and c) TSMC method.

4.1 Step Change in the Output Reference Voltage

In this study, the reference voltage magnitude is suddenly decreased to half of the nominal value at t = 0.15 s and returns to the nominal value at t = 0.25 s. At the top of Fig. 6, V_{ref} and V_{out} root mean square (RMS) values are depicted, exhibiting how the reference voltage is followed by the output voltage. At

Table 1 CDFIG Parameters.

Parameter	Value
V	220 V
R_{s1}	1.6 Ω
R_{s2}	1.6 Ω
R_r	3.2 Ω
R_L	400 Ω
$p1$	1
$p2$	1
L_{ls1}	0.004 H
L_{ls2}	0.004 H
L_{lr}	0.008 H
L_m	0.125 H

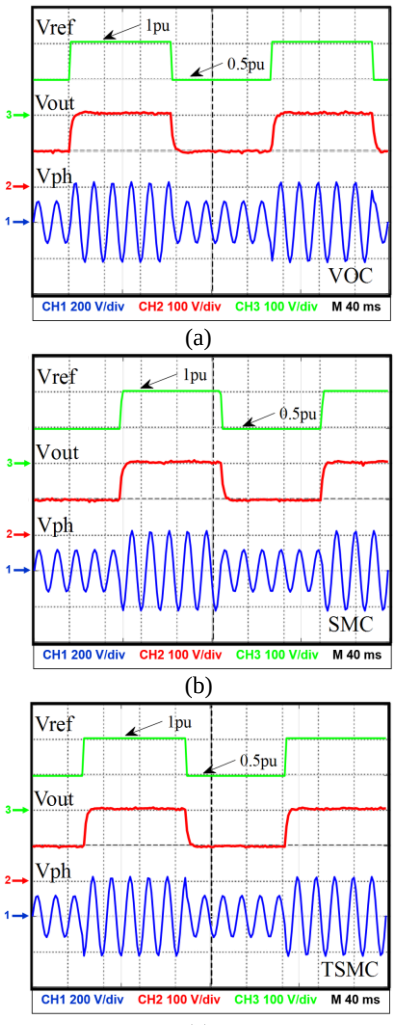

Fig. 7 Experimental change reference of voltage; a) VOC method, b) SMC method, and c) TSMC method.

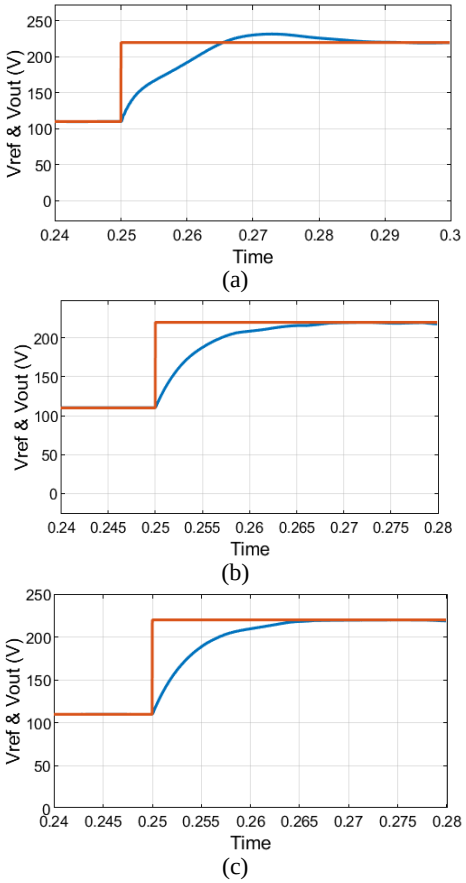

Fig. 8 Simulation dynamic response to changes in the ref1erence value, V_{ref} (red), V_{out} (blue); a) VOC method, b) SMC method, and c) TSMC method.

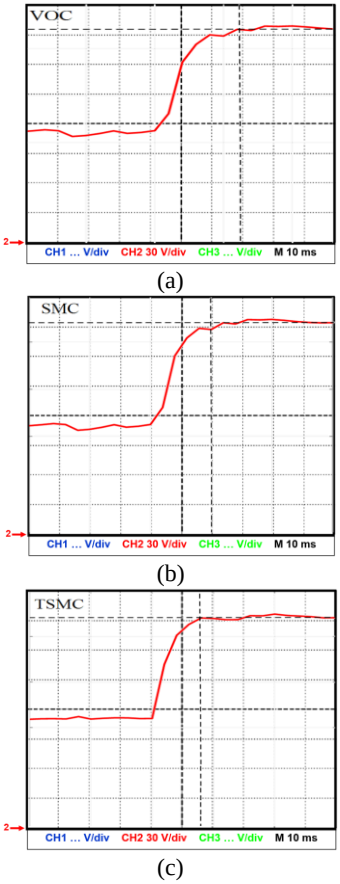

Fig. 9 Experimental dynamic response to changes in the reference value of voltage, a) VOC method, b) SMC method, and c) TSMC method.

the bottom of Fig. 6, the three-phase voltage of the load is depicted.

The output voltage properly follows the reference voltage. According to the simulation results in Fig. 5, the total harmonic distortion (THD) of the output voltage is about 2.5%, 2%, and 1.5% for VOC, SMC, and TSMC, respectively. Moreover, according to the experimental results in Fig. 7, the THD of the output voltage is about 3%, 2.5%, and 2% for VOC, SMC, and TSMC methods, respectively.

In order to verify the dynamic response of the studied controllers, the output reference voltage amplitude is changed from 110 V to 220 V and the responses are shown in Figs. 8 and 9 for simulation and experimental tests, respectively. It is observed that the response time in TSMC is below 15 ms while in the SMC is 20 ms and in VOC is 40 ms.

4.2 Change in Rotor Speed

In order to show the robustness of the proposed method to rotor speed, the prime mover's speed is changed from 4000 to 3500 rpm at 0.15 sec with ramp shape and then is increased to 4000 rpm again at 0.25 sec. with ramp shape. Fig. 10 shows that, during the speed variation, the PM output voltage and frequency are controlled, but the CM current frequency decreases proportional to the CDFIG slip changes. The experimental results are shown in Fig. 11.

Therefore, the proposed SMC and TSMC have proven to be robust to rotor speed variations. The comparison results are summarized in Table 2.

4.3 Nonlinear Load

Various nonlinear loads such as power supplies and electronic ballasts are used in domestic and office applications. These loads impose high current harmonic distortions which distort the terminal voltage. In order to show the performance of control methods to derive the nonlinear load, a 3-phase diode bridge rectifier, which supplies an electrolyte capacitance paralleled with resistance load, is connected to the terminal of the power machine, as shown in Fig. 12.

This test is the investigation of the control methods with a combination of linear and nonlinear loads. In Fig. 13, the output voltage amplitude, the phase voltage, and output current of the CDFIG are shown. The PM output current is nonlinear while the TSMC keeps the output voltage closely sinusoidal and it follows the reference voltage. Experimental results are shown in Fig. 13.

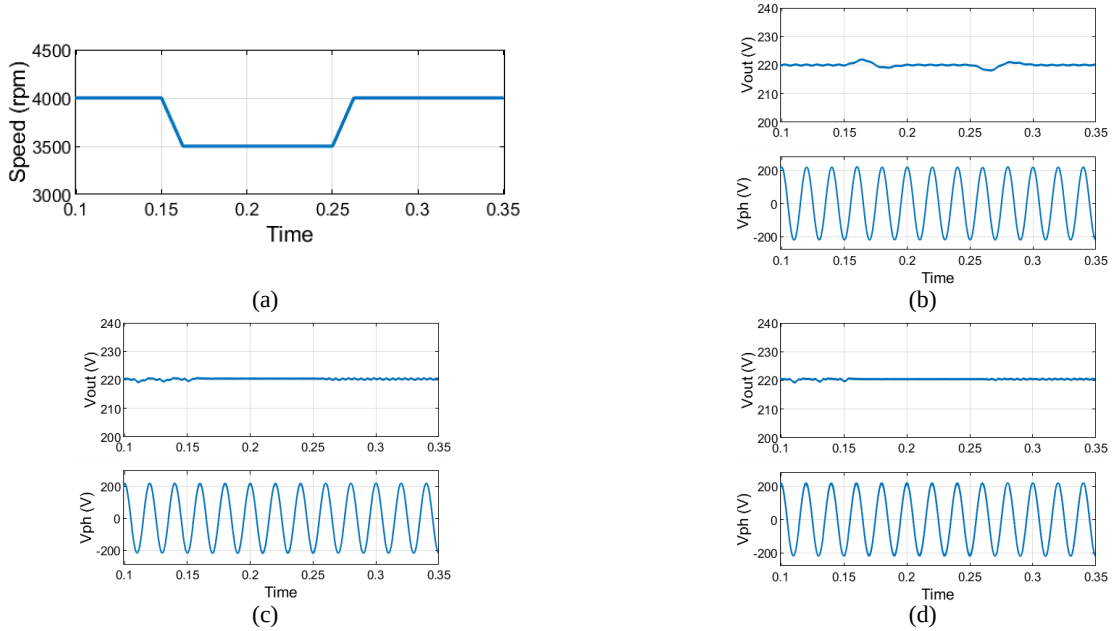

Fig. 10 Simulation dynamic response to changes in the rotor speed and the generated voltage of power machine; a) prime mover's speed, b) VOC, c) SMC, and d) TSMC.

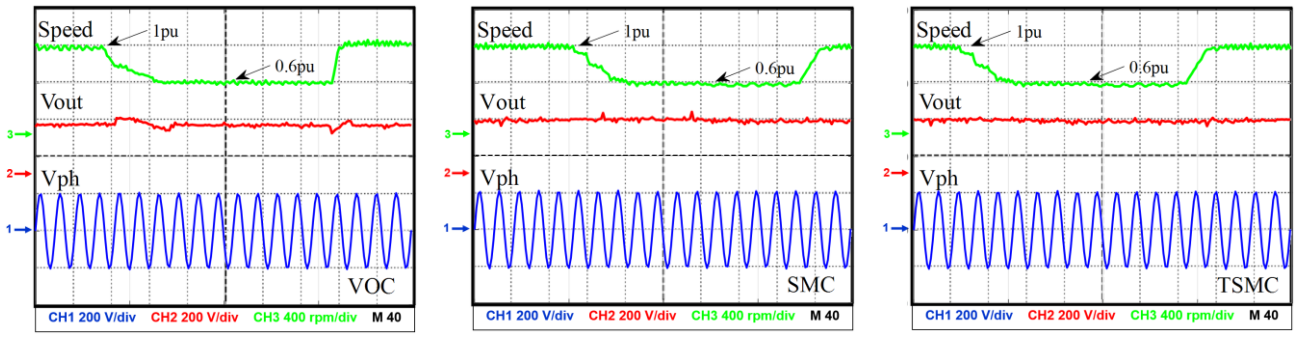

Fig. 11 Experimental result for speed change; speed (green), output voltage (red), and phase voltage (blue).

Table 1 Comparison results.

Control Method	VOC	SMC	TSMC
THD Simulation	2.5%	2%	1%
THD Experimental	3%	2.5%	2%
Response time	40 ms	20 ms	15 ms

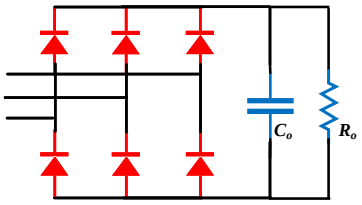

Fig. 12 Nonlinear load (3-ph bridge rectifier).

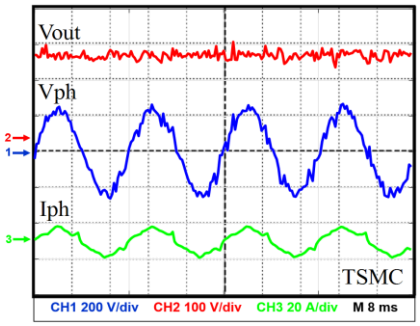

Fig. 13 Experimental result for nonlinear load based on TSMC; output voltage amplitude (red), phase voltage (blue), load current (green).

The comparison between simulation results of control methods for the nonlinear load is presented in Fig. 14. As can be seen, the reference voltage magnitude is suddenly decreased to half of the nominal value at $t = 0.15$ s and the load voltage and its current are depicted in Fig. 14. The chattering phenomenon is seen on the SMC response, while in TSMC the chattering is less than the conventional mode. As well as, the results of the VOC method has no perturbation like as chattering, but the dynamic response is lower than

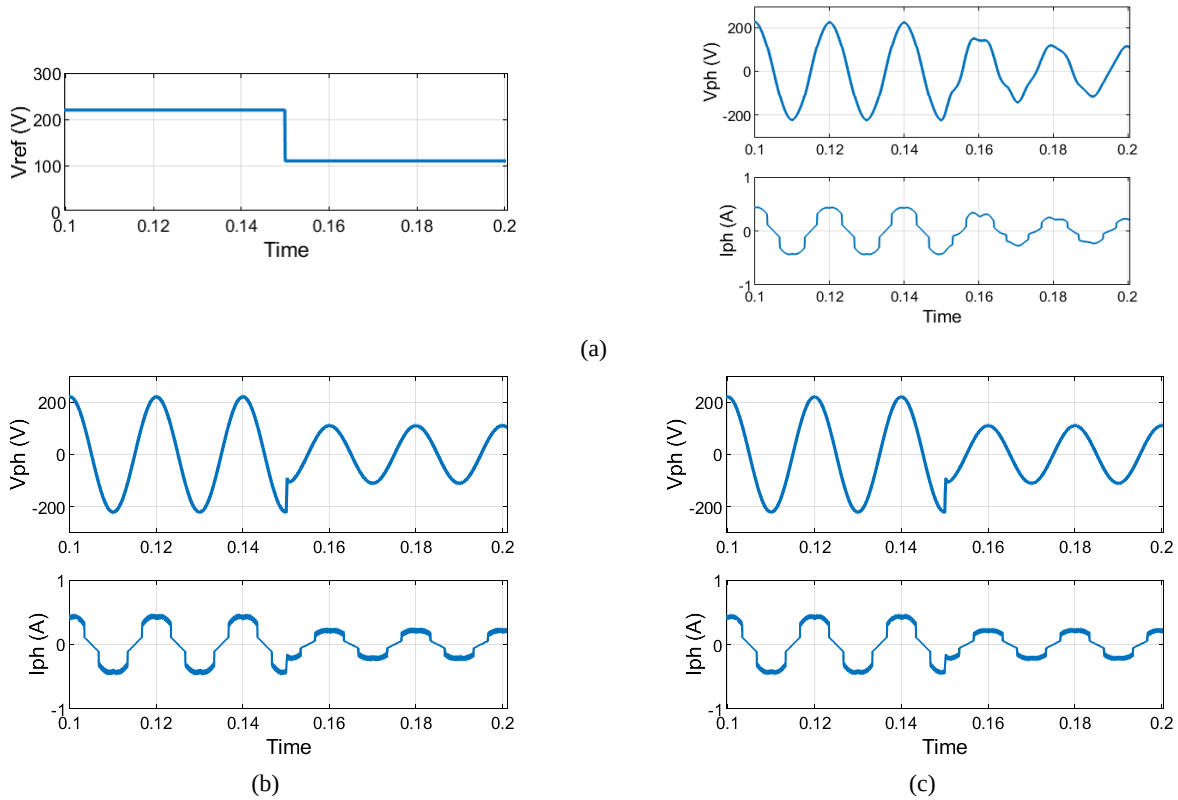

Fig. 14 Simulation results for nonlinear load with a step change in output voltage; output voltage and output current; a) VOC, b) SMC, and c) TSMC.

sliding mode based methods.

5 Conclusion

In this paper, the variable structure controller called as TSMC is developed and applied to CDFIG. The performance of the TSMC is evaluated and compared with conventional VOC and the regular SMC methods in the context of voltage control of the generator for linear and nonlinear loads. Simulation and experimental results show that the VOC technique is affected by changes in the speed and load whereas the SMC and TSMC techniques are robust to such parameter variations/uncertainties. Moreover, the TSMC has faster dynamic responses compared to the VOC and SMC methods. In addition, when the load is nonlinear, the TSMC causes lower output distortion than the SMC and VOC controllers. Detailed simulation results using MATLAB/Simulink software and experimental results using a DSP-based inverter setup are presented.

References

[1] Z. Gao, C. Tang, X. Zhou, and Y. Ma, "An overview about VSCF and LVRT in wind power generation," in *29th Chinese Control And Decision Conference (CCDC)*, Chongqing, pp. 554–558, 2017.

[2] F. Blaabjerg, M. Liserre, and K. Ma, "Power electronics converters for wind turbine systems," *IEEE Transactions on industry applications*, Vol. 48, No. 2, pp. 708–719, 2012.

[3] B. Hopfensperger, D. J. Atkinson, and R. A. Lakin, "Stator flux oriented control of a cascaded doubly-fed induction machine," *IEE Proceedings-Electric Power Applications*, Vol. 146, No. 6, pp. 597–605, Nov. 1999.

[4] T. D. Strous, H. Polinder, and J. A. Ferreira, "Brushless doubly-fed induction machines for wind turbines: developments and research challenges," in *IET Electric Power Applications*, Vol. 11, No. 6, pp. 991–1000, 7 2017.

[5] E. Abdi, R. McMahon, P. Malliband, S. Shao, M. E. Mathekga, P. Tavner, S. Abdi, A. Oraee, T. Long, and M. Tatlow, "Performance analysis and testing of a 250 kW medium-speed brushless doubly-fed induction generator," *IET Renewable Power Generation*, Vol. 7, No. 6, pp. 631–638, 2013.

[6] M. El Achkar, R. Mbayed, G. Salloum, S. Le Ballois, and E. Monmasson, "Generic study of the power capability of a cascaded doubly fed induction machine," *International Journal of Electrical Power & Energy Systems*, Vol. 86, pp. 61–70, 2017.

[7] S. Ademi, M. Jovanovic, and M. Hasan, "Control of brushless doubly-fed reluctance generators for wind energy conversion systems," *Transactions on Energy Conversion*, Vol. 30, No. 2, pp. 596–604, 2015.

[8] Y. Tang, H. He, Z. Ni, J. Wen, and X. Sui, "Reactive power control of grid-connected wind farm based on adaptive dynamic programming," *Neurocomputing*, Vol. 125, pp. 125–133, 2014.

[9] J. Chen, W. Zhang, B. Chen, and Y. Ma, "Improved vector control of brushless doubly fed induction generator under unbalanced grid conditions for offshore wind power generation," *IEEE Transactions on Energy Conversion*, Vol. 31, No. 1, pp. 293–302, 2015.

[10] I. Yaichi, A. Semmah, P. Wira, and S. M. ElAmine, "An improved direct power control based on SVM strategy of the doubly fed induction generator," in *7th International Renewable and Sustainable Energy Conference (IRSEC)*, Agadir, Morocco, pp. 1–8, 2019.

[11] J. de Dieu Nguimfack-Ndongmo, G. Kenné, R. Kuate-Fochie, A. Cheukem, H. B. Fotsin, and F. Lamnabhi-Lagarrigue, "A simplified nonlinear controller for transient stability enhancement of multimachine power systems using SSSC device," *International Journal of Electrical Power & Energy Systems*, Vol. 54, pp. 650–657, 2014.

[12] G. D. Wang, R. J. Wai, and Y. Liao, "Design of back stepping power control for grid-side converter of voltage source converter-based high-voltage dc wind power generation system," *IET Renewable Power Generation*, Vol. 7, No. 2, pp. 118–133, 2013.

[13] H. E. Medouce, H. Benalla, A. Mehdi, and A. Reama, "Sensorless direct power regulation by sliding mode approach of DFIG generator based wind energy system," in *IEEE 15th International Conference on Environment and Electrical Engineering (EEEIC)*, Rome, pp. 1880–1885, 2015.

[14] B. Beltran, M. E. H. Benbouzid, and T. Ahmed-Ali, "Second-order sliding mode control of a doubly fed induction generator driven wind turbine", *IEEE Transactions on Energy Conversion*, Vol. 27, No. 2, pp. 261–269, 2012.

[15] Z. TIR, H. Rajeai, and R. Abdessemed, "Analysis and vector control of a cascaded doubly fed induction generator in wind energy applications," *Revue des Energies Renouvelables SMEE'10*, pp. 347–358, 2010.

[16] M. E. Achkar, R. Mbayed, G. Salloum, N. Patin, S. Le Ballois, and E. Monmasson, "Modeling and control of a standalone cascaded doubly fed induction generator supplying an isolated load," in *17th European Conference on Power Electronics and Applications (EPE'15 ECCE-Europe)*, Geneva, pp. 1–10, 2015.

[17] Z. S. Du and T. A. Lipo, "Dynamics and vector control of wound-rotor brushless doubly fed induction machines," in *IEEE Energy Conversion Congress and Exposition (ECCE)*, Pittsburgh, PA, pp. 1332–1339, 2014.

[18] J. Hu, J. Zhu, and D. G. Dorrell, "A new control method of cascaded brushless doubly fed induction generators using direct power control," in *IEEE Transactions on Energy Conversion*, Vol. 29, No. 3, pp. 771–779, Sep. 2014.

[19] R. P. Vieira, L. T. Martins, J. R. Massing, and M. Stefanello, "Sliding mode controller in a multiloop framework for a grid-connected VSI with LCL filter," *IEEE Transactions on Industrial Electronics*, Vol. 65, No. 6, pp. 4714–4723, Jun. 2018.

[20] S. K. Pandey, S. L. Patil, and S. B. Phadke, "Comment on "PWM-based adaptive sliding-mode control for boost DC-DC converters" [Aug 13, 3291-3294]," *IEEE Transactions on Industrial Electronics*, Vol. 65, No. 6, pp. 5078–5080, Jun. 2018.

[21] I. M. Hassine, M. W. Naouar, and N. Mrabet-Bellaaj, "Model predictive-sliding mode control for three-phase grid-connected converters," *IEEE Transactions on Industrial Electronics*, Vol. 64, No. 2, pp. 1341–1349, Feb. 2017.

[22] S. T. Venkataraman and S. Gulati, "Control of nonlinear systems using terminal sliding modes", in *Proceedings of the 1992 American Control Conference*, Chicago, USA, pp.891–893, 1992.

[23] İ.Yazici and E. K. Yaylaci, "Fast and robust voltage control of DC-DC boost converter by using fast terminal sliding mode controller," *IET Power Electronics*, Vol. 9, No. 1, pp. 120–125, 2016.

[24] J. J. E. Slotine and W. Li, *Applied nonlinear control*. Englewood Cliffs, NJ: Prentice-Hall, 1991.

[25] X. Yu and M. Zhihong, "Fast terminal sliding-mode control design for nonlinear dynamical systems," *IEEE Transactions on Circuits and Systems I: Fundamental Theory and Applications*, Vol. 49, No. 2, pp. 261–264, Feb. 2002.

H. Zahedi Abdolhadi received the B.Sc. degree in Electrical Engineering from the University of Kashan, Kashan, Iran, in 2007 and the M.Sc. degree in Electrical Engineering from Tarbiat Modares University, Tehran, Iran, in 2010. He is currently working toward the Ph.D. degree in the Faculty of Engineering, Shahrekord University, Shahrekord, Iran. His research interests include power converters, motor drivers and nonlinear control as well as control of power electronics and electric drives using microcontrollers and DSPs.

Gh. Arab Markadeh received the B.Sc., M.Sc., and Ph.D. degrees in Electrical Engineering from Isfahan University of Technology, Iran, in 1996, 1998, and 2005, respectively. He is currently an Associate Professor in the Faculty of Engineering, Shahrekord University. His fields of research include nonlinear control, power electronics, and variable-speed drives. He is the Editor-in-chief of Journal of Dam and Hydroelectric Powerplant. Dr. Arab Markadeh was the recipient of the IEEE Industrial Electronics Society IECON'04 best paper presentation award in 2004.

S. Taghipour Boroujeni received the B.Sc., M.Sc., and Ph.D. degrees in Electrical Engineering from the Department of Electrical Engineering, Amirkabir University (Tehran Polytechnic), Tehran, Iran, in 2003, 2005, and 2009, respectively. In 2009, he joined the Department of Engineering, Shahrekord University, Shahrekord, Iran, as an Assistant Professor. Since 2016, he has been working as an Associate Professor. His research interests include modeling, design, analysis, optimization, and control of electrical machines, especially variable-speed generators.